EXPERIMENTS AND MODELING OF DILUTION JET FLOW FIELDS

James D. Holdeman
NASA Lewis Research Center
Cleveland, Ohio

This paper presents experimental and analytical results of the mixing of single, double, and opposed rows of jets with an isothermal or variable-temperature main stream in a straight duct. This study was performed to investigate flow and geometric variations typical of the complex, three-dimensional flow field in the dilution zone of gas-turbine-engine combustion chambers.

The principal results, shown experimentally and analytically, were the following: (1) variations in orifice size and spacing can have a significant effect on the temperature profiles; (2) similar distributions can be obtained, independent of orifice diameter, if momentum-flux ratio and orifice spacing are coupled; (3) a first-order approximation of the mixing of jets with a variable-temperature main stream can be obtained by superimposing the main-stream and jets-in-an-isothermal-crossflow profiles; (4) the penetration of jets issuing from slanted slots is similar to that of jets from circular holes, but the mixing is slower and is asymmetric with respect to the jet centerplanes, which shift laterally with increasing downstream distance, (5) double rows of jets give temperature distributions similar to those from a single row of equally spaced, equal-area circular holes; (6) for opposed rows of jets, with the orifice centerlines in line, the optimum ratio of orifice spacing to duct height is one-half the optimum value for single-side injection at the same momentum-flux ratio; and (7) for opposed rows of jets, with the orifice centerlines staggered, the optimum ratio of orifice spacing to duct height is twice the optimum value for single-side injection at the same momentum-flux ratio.

In illustrating these results, the mean temperature measurements are compared with profiles calculated using an empirical model based on assumed vertical profile similarity and superposition and with distributions calculated using a three-dimensional elliptic code that had a standard k-ε turbulence model. The empirical model predictions are very good within the range of the generating experiments, and the numerical model results, although they exhibit too little mixing, correctly describe the effects of the principal flow and geometric variables.

SYMBOLS

A_j/A_m jet to main-stream area ratio, $A_j/A_m = (\pi/4)/[(S/H_0)(H_0/D)^2]$ for one-side injection and $(\pi/2)/[(S/H_0)(H_0/D)^2]$ for two-side injection

C $(S/H_0)\sqrt{J}$, eq. (3)

C_d orifice discharge coefficient

D orifice diameter

D_j $D\sqrt{C_d}$

DR jet to main-stream density ratio, DR $\cong T_m/T_j$

H_0 duct height

J jet to main-stream momentum-flux ratio, J = $(DR)R^2$

M jet to main-stream mass-flux ratio, M = (DR)R

R jet to main-stream velocity ratio, R = V_j/U_m

S spacing between orifice centers

S_x spacing between orifice rows

T temperature

T_j jet exit temperature

T_m main-stream temperature

U velocity

U_m main-stream velocity

V_j jet velocity

$W^{+}_{1/2}$ jet half-widths above (+) or below (-) the centerline (ref. 5)

w_j/w_T jet to total mass-flow ratio, $w_j/w_T = \sqrt{(DR)J}\,(C_d)(A_j/A_m)/\left(1 + \sqrt{(DR)J}\,(C_d)(A_j/A_m)\right)$

x downstream coordinate (x = 0 at injection plane)

y cross-stream (radial) coordinate (y = 0 at wall; y = y_c at location of minimum temperature in a line x = constant and z = constant)

z lateral (circumferential) coordinate (z = 0 at centerplane)

θ $(T_m - T)/(T_m - T_j)$, eq. (1)

θ_c temperature difference ratio at y_c

$\theta^{\pm}_{min}$ minimum temperature difference ratio above (+) or below (-) the centerline, (fig. 4)

INTRODUCTION

The problem of jets in crossflow has been rather extensively treated in the literature, to the point that it can almost be called a classical three-dimensional flow problem. Although these studies have all contributed to the understanding of the general problem, the information obtained in any given

study is naturally determined by the motivating application and therefore may not satisfy the specific needs of diverse applications.

Consideration of dilution zone mixing in gas-turbine combustion chambers has motivated several previous studies of the mixing characteristics of jets injected normally into a ducted crossflow (refs. 1 to 12). One factor making the combustor dilution zone jet-in-crossflow application unique is that it is a confined mixing problem - 10 to 50 percent of the total flow enters through the dilution jets. The result is that the equilibrium temperature of the exiting flow may differ significantly from that of the entering main-stream flow. To control or tailor the combustor exit temperature pattern, we must be able to characterize the exit distribution in terms of the upstream flow and geometric variables. This requires that the entire flow field be either known or modeled.

Empirical correlation of experimental data can provide an excellent predictive capability within the parameter range of the generating experiments (e.g., refs. 4 to 6), but empirical models must be used with caution, or not at all, outside this range. Physical modeling, in various levels of sophistication and complexity, may be used to obviate this weakness. In this regard, several one- and two-dimensional, integral and differential jet-in-crossflow models have been developed and shown to give, for example, trajectory predictions that are in good agreement with experiments. These models may provide insight into the dominant physical mechanism(s) and may predict some of the characteristic parameters well, but they rarely provide sufficient information to quantify the flow field in three coordinate directions.

Recently, rapid advances have been made in the capability of computational fluid dynamics models and in their application to complex flows such as jets in crossflow (refs. 13 to 16). These models are, however, still in the development and verification stage. They have been shown to be capable of predicting trends in complex flows, but their capability to provide accurate, quantitive, and grid-independent calculations of these flows has not yet been demonstrated (refs. 14 to 16).

PREVIOUS RESULTS AND THE CURRENT STUDY

The study in references 17 to 19 was performed to extend the available experimental data on, and the empirical correlations of, the thermal mixing of multiple jets in crossflows so that they would include geometric and flow variations characteristic of gas turbine combustion chambers - namely, variable temperature main stream, flow area convergence, noncircular orifices, and double and opposed rows of jets. These experiments are a direct extension of those in reference 1. The effect on the dimensionless temperature distributions of varying the jet to main-stream density ratio, the momentum-flux ratio, and the orifice size and spacing are presented in reference 2.

From the data in reference 1, an empirical model was developed (refs. 4 and 5) for predicting the temperature field downstream of a row of jets mixing with a confined crossflow. The effects of separately varying the independent flow and geometric variables and the relations among these variables which optimize the mixing are reviewed in reference 12. This study was conducted using an interactive microcomputer program that is based on the empirical model of reference 5.

The results of these investigations may be summarized as follows: (1) mixing improves with increasing downstream distance; (2) the momentum-flux ratio is the most significant flow variable; (3) the effect of density ratio is small at constant momentum-flux ratio; (4) at any given momentum-flux ratio, decreasing orifice spacing while maintaining a constant orifice diameter reduces penetration and increases lateral uniformity; (5) increasing orifice diameter while maintaining a constant spacing-to-diameter ratio improves penetration but increases lateral nonuniformity; (6) increasing orifice diameter at a constant orifice spacing increases the magnitude of the temperature difference, but jet penetration and profile shape remain similar; (7) profiles for conditions with equivalent coupling of orifice spacing and momentum-flux ratio show similar distributions; and (8) smaller momentum-flux ratios (larger spacing) require a greater downstream distance for equivalent mixing.

Results from the experiments in references 17 to 19 that are considered in this paper include the effects of variations in orifice size and spacing, coupled spacing and momentum-flux ratio, variable temperature main stream, noncircular orifices, and double and opposed rows of inline and staggered jets. Also, temperature field measurements from several experiments are compared with distributions calculated using an empirical model based on assumed vertical profile similarity and superposition (refs. 17 to 19) and using a three-dimensional elliptic code with a standard k-ε turbulence model (ref. 14). The results show the capability of these models to predict the effects of the principal flow and geometric variables.

A more complete presentation of the experimental results and a discussion of the empirical modeling performed in this study are given in references 1, 4, and 17 to 19. Selected experimental and analytical results from these studies and from reference 14 are also given in references 2, 5, and 20 to 23.

FLOW FIELD DESCRIPTION

Figure 1 shows a schematic of the dilution jet flow field for jet injection from the top wall. The temperature field results are presented in three-dimensional oblique views of the temperature difference ratio θ:

$$\theta = \frac{T_m - T}{T_m - T_j} \tag{1}$$

A sequence of experimental profiles of this parameter at several locations downstream of the injection plane is shown in figure 2. In the three-dimensional plots the temperature distribution is shown in the y,z-planes normal to the main flow direction x. The coordinates y and z are, respectively, normal and parallel to the orifice row. Note that the jet fluid is identified by the larger values of the θ parameter (i.e., $\theta = 1$ if $T = T_j$, and $\theta = 0$ if $T = T_m$). The equilibrium θ for any configuration is equal to the fraction of the total flow entering through the dilution jets w_j/w_T.

The orifice configurations investigated are shown in figure 3. The primary independent geometric variables for each orifice configuration are the spacing between adjacent orifices S, the orifice diameter D (for noncircular orifices, this is taken as the diameter of a circle of equal area), and, for double rows, the axial spacing between rows S_x. These are expressed in

dimensionless form as the ratio of the orifice spacing to duct height S/H_0, the ratio of the duct height to orifice diameter H_0/D, and the ratio of the axial spacing to the duct height S_x/H_0.

EXPERIMENTAL CONSIDERATIONS

The dilution-jet mixing characteristics were determined by measuring temperature and pressure distributions with a vertical-rake probe positioned at different axial and lateral stations. This probe had 20 thermocouple elements. A 20-element total-pressure rake and a 20-element static-pressure rake were located nominally 5 mm ($0.05\ H_0$) on each side of the thermocouple rake. The center-to-center spacing between sensors on each rake was $0.05\ H_0$.

This probe traversed a matrix of 48 to 64 z,x-plane survey locations. The flow field was mapped in the z-direction over a distance of 1 or 1.5 times the hole spacing S at intervals of S/10. For most tests, the x,y-plane containing the orifice centerline (centerplane) was at the center of the span surveyed; that is, data surveys were from midplane to midplane.

Measurements in the x-direction were made at up to five planes with $0.25 < X/H_0 < 2$. Because the objective in this application is to identify dilution-zone configurations that will provide a desired mixing pattern within a given combustor length, the downstream stations are defined in intervals of the duct height H_0 rather than intervals of the orifice diameter D.

FLOW FIELD MODELS

Empirical

The empirical model for the temperature field downstream of jets mixing with a confined crossflow is based on the observation that properly nondimensionalized vertical temperature profiles can be expressed in the following self-similar form (ref. 5) for any location in the flow field:

$$\frac{\theta - \theta_{\overline{min}}^{+}}{\theta_c - \theta_{\overline{min}}^{+}} = \exp\left[- \ln 2 \ \frac{(y - y_c)^2}{W_{1/2}^{+}} \right] \tag{2}$$

where θ is the temperature difference ratio at vertical location y, and θ_{min}^{+}, θ_{min}^{-}, $W_{1/2}^{+}$, $W_{1/2}^{-}$, θ_c, and y_c are scaling parameters as shown in figure 4. Correlations have been developed for each of these in terms of the independent variables J, S/D, H_0/D, Z/S, and x/H_0. The correlations in reference 5 for a single row of jets in a uniform temperature crossflow have been extended for predicting the temperature field downstream of single, double, or opposed rows of jets, either inline or staggered, injected into an isothermal or nonisothermal main stream, with or without flow-area convergence (refs. 17 to 19).

Numerical

The numerical code used in this investigation is based on the USARTL three-dimensional, fully elliptic, turbulent flow model (ref. 24) and uses pressure and velocity as the main hydrodynamic variables. This code, or similar versions thereof, has been used in previous validation and assessment studies (refs. 14 to 16).

The governing equations are represented by finite-difference approximations on a staggered grid system. The differencing technique employed is hybrid for convective terms with central differencing of all other terms. The velocity-pressure coupling is handled by the SIMPLE algorithm of Patankar and Spalding (refs. 25 and 26). Uniform velocities and mass flow rates were used at all inflow boundaries. The code contained a conventional $k-\varepsilon$ turbulence model, and standard values of the constants C_D, C_1, and C_2 were used (i.e., $C_D = 0.09$, $C_1 = 1.44$, $C_2 = 1.92$). The rms turbulence intensity was chosen to be 4.5 percent of the local mean velocity, the inlet length scale was 2 percent of the jet diameter and duct height for the jet and main stream, respectively, and the turbulent Prandtl number was 0.9 for all calculations.

RESULTS AND DISCUSSION

The following paragraphs describe the experimental results and compare them with those of the empirical and numerical model calculations, and illustrate the effects of the primary independent variables. The flow and geometry conditions corresponding to the figures shown are given in table I.

Orifice Size and Spacing

At constant orifice area, changes in orifice size and spacing can have a significant influence on the θ profiles. This is shown by the experimental profiles in figure 5 where jets from closely spaced small orifices underpenetrate and remain near the injection wall (fig. 5(a)), and jets from widely spaced larger orifices overpenetrate and impinge on the opposite wall (fig. 5(b)). In this figure, and in several others in which the orifice spacing is different for different parts of the figure, a duct cross-section is included to indicate the region for which data are shown.

The data for these conditions, at $x/H_0 = 0.5$, are compared with calculated distributions in figure 6. The empirical model reproduces the data very well in the small orifice case because the data are consistent with the major assumption in the empirical model, namely that all vertical temperature distributions can be reduced to similar Gaussian profiles. The empirical model does not do as well in the larger orifice case, however, because the impingement of the jets on the opposite wall results in vertical profiles which are not similar.

The numerical model calculations were made with approximately 20 000 nodes. Although these are in qualitative agreement with the data, they show temperature gradients that are too steep, especially in the transverse direction. Underprediction of the mixing was also seen in the single-jet calculations of reference 13 where it is shown that the $k-\varepsilon$ type of turbulence model

underestimates the intensity. The result in figure 6 is typical of the numerical model calculations shown in this paper.

For the small-orifice case a coarse-grid calculation using less than 6000 nodes was also performed. This calculation is shown on the right side of figure 6(a) and illustrates the significant influence that grid selection can have on the solution obtained, and the smearing of the profiles which can occur as a result of numerical diffusion.

Coupled Spacing and Momentum-Flux Ratio

Examination of the experimental data revealed that similar jet penetration is obtained, independent of orifice diameter, if orifice spacing and momentum-flux ratio are coupled (refs. 2, 5, 12, and 22). For example, low momentum-flux ratios require large, widely spaced holes, whereas smaller, closely spaced holes are appropriate for high-momentum flux ratios, as shown in figure 7. The duct cross section is shown to the right of the three-dimensional oblique and isotherm contour plots for each configuration. It follows that for low momentum-flux ratios (large spacing) a greater axial distance is required for equivalent mixing.

In general, jet penetration and centerplane profiles are similar when the orifice spacing and the square root of the momentum-flux ratio are inversely proportional; that is,

$$C = (S/H_0)\sqrt{J} \tag{3}$$

For single-side injection, the centerplane profiles are approximately centered across the duct height and approach an isothermal distribution in the minimum downstream distance when $C = 2.5$. This appears to be independent of orifice diameter, as shown in both the calculated and experimental profiles in figure 8. In equation (3), values of C that are a factor of 2 or more smaller or larger than the optimum values correspond to underpenetration or overpenetration, respectively. (Figs. 5 and 6 and table I). A summary of the spacing and momentum-flux ratio relationships for single-side injection is given in table II.

Variable Temperature Main Stream

The influence of a nonisothermal main-stream flow on measured profiles for intermediate momentum-flux ratios with $S/H_0 = 0.5$ and $H_0/D = 4$ is shown in figure 9. The corresponding isothermal main-stream case is shown in the top row. In the center row of the figure, the upstream profile (left frame) is coldest near the injection wall, whereas in the bottom row, the upstream profile (left frame) is coldest near the opposite wall. For the definition of θ in this figure, T_m is the hottest temperature in the main stream for each case.

Experimental, empirical, and numerical results for the top-cold case are shown in figure 10. The empirical calculations are from a superposition of the upstream profile and the corresponding jets-in-an-isothermal-main-stream distribution (ref. 22). Although this gives a good first-order approximation, it should be noted that with a variable temperature main stream there can be

cross-stream thermal transport due to the flow of main-stream fluid around the jets (and hence, to different y locations), and this is not accounted for when the distributions are superimposed. This becomes apparent if the local main-stream temperature $T_m(y)$, is used in the definition of θ in equation (1).

In the variable temperature main-stream case, the numerical model results agree well with the experimental data, especially on the jet centerplane, but the transverse mixing is underpredicted, as in the corresponding isothermal main-stream case shown in figure 8(b).

Slanted Slots

Figure 11 shows experimental and calculated three-dimensional oblique θ distributions for slanted slots at intermediate momentum-flux ratios. These slots had an aspect ratio (length/width) of 2.8, with their major axes slanted at 45° to the main-stream flow direction. The orifice spacing and size are $S/H_0 = 0.5$ and $H_0/D = 4$, respectively. The temperature distributions in this figure may be compared with those for equivalent-area circular holes in figure 8(b). As noted in reference 23, the penetration and mixing of jets from the slanted slots are noticeably less than those of jets from the circular holes. The normally symmetric vortex pair is asymmetric in this case, as is apparent in the experimental profiles in figure 11 (and in the figures in ref. 23). These profiles also show that the centerplanes of the jets shift laterally with increasing downstream distance.

The empirical model calculations include a modification to account for the observed centerplane shift, but they do not model the asymmetry (refs. 19 and 23). The numerical calculations for this case exhibit both the centerplane shift and the asymmetry, and they are good in the context of the qualitative agreement seen throughout the comparisons given in this paper.

Double Rows of Holes

Figure 12 shows experimental and calculated temperature distributions for an orifice plate with two inline rows of jets ($S_x/H_0 = 0.5$) from circular orifices. It was observed from the experimental profiles in reference 23 that the two configurations have very similar temperature distributions, and this is seen in the calculated profiles as well. In this case the empirical model calculations are derived by superimposing the distributions from the two rows.

Both experimental and calculated temperature distributions are shown in figure 13 for a double-row configuration when $S_x/H_0 = 0.25$ and the trailing row has twice as many orifices as the lead row. Note that the orifice area is the same for both rows. These profiles show the dominance of the lead row in establishing the jet penetration and first-order profile shape (ref. 23). As with the double row of inline holes, the empirical calculations for this case were obtained by superimposing separate calculations for the two rows.

Opposing Rows of Jets

The remainder of this paper presents results for two-side injection from opposing rows of jets with (1) the top and bottom jet centerlines directly opposite each other and (2) the top and bottom jet centerlines staggered in the z direction. The experimental results are shown and compared with the single-side results in figures 14 and 16. In these figures, a duct cross section, drawn to scale, is to the left of the data.

Opposed Rows of Inline Jets

Figure 14 shows a comparison at intermediate momentum-flux ratios for single-side and opposed-jet injection. For these momentum-flux ratios, an appropriate orifice-spacing-to-duct-height ratio for optimum single-side mixing is approximately 0.5 (see eq.(2)), as confirmed by the profiles in figure 7.

For opposed-jet injection, with equal momentum-flux ratios on both sides, the effective mixing height is half the duct height because, as reference 3 shows, the effect of an opposite wall is similar to that of the plane of symmetry in an opposed-jet configuration. Thus, the appropriate orifice-spacing-to-duct-height ratio for opposed-jet injection at these intermediate momentum-flux ratios would be about $S/H_0 = 0.25$. Dimensionless temperature distributions downstream of jets with this spacing are shown in the bottom row of figure 14, and the two streams do indeed mix very rapidly. Note that since the orifices in figures 14(a) and (b) are the same size, the jet to main-stream flow ratio is four times greater for opposed-jet injection than for single-side injection. If it is desired to maintain an equal flow rate, the orifice diameter must be halved, since there is injection from both sides and opposed-jet injection requires twice as many holes in the row as optimum single-side injection.

Figure 15 shows experimental and calculated profiles for opposed rows of jets with identical orifice spacing and diameter and with the orifice centerlines in line. The empirical model predicts opposed-jet injection very well, as the experimental profiles on both sides of the plane of symmetry support the Gaussian profile assumption. The penetration and profile shape calculated with the numerical model are in good agreement with the data, but the mixing is otherwise underpredicted, as evidenced by the steep transverse and lateral gradients seen in almost all the previous calculations also.

Opposed Rows of Staggered Jets

Figure 16 shows comparisons of single-side and staggered jet injection for intermediate momentum-flux ratios. Since the effective mixing height for opposed inline injection was half the duct height, it was assumed that the effective orifice spacing for staggered jets would be half the actual spacing. Thus, to maintain an optimum coupling of the effective spacing and the momentum-flux ratio, the orifice spacing for opposed staggered configurations should be double that which is appropriate for single-side injection.

This hypothesis is verified by the rapid mixing of the two streams in the bottom row of profiles in figure 16. This figure shows clearly that a config-

uration which mixes well with one-side injection performs even better when every other orifice is moved to the opposite wall.

Empirical and numerical model calculations for an opposed row of staggered jets are compared with the data in figure 17. The empirical model does not handle this complex case well, as the fluid dynamic interactions here are not amenable to a direct extension of the simple Gaussian profile and superposition type of modeling appropriate for most of the single-side and opposed-jet cases of interest. The numerical model calculations are not in appreciably better agreement with the data than are the empirical model results, however, because the mixing is underpredicted here as in the previous cases.

A summary of the spacing and momentum-flux ratio relationships which give optimum mixing for opposed rows of inline and staggered jets is given in table II.

LIMITATIONS AND APPLICABILITY

Empirical

The empirical model results presented here show that correlating experimental data can provide an excellent predictive capability within the parameter range of the generating experiments, provided the experimental results are consistent with the assumptions made in the empirical model. These models must, however, be used with caution, or not at all, outside this range.

The ranges of the experimental variables on which this empirical model was based are given in table III. The density ratio, momentum-flux ratio, orifice spacing, and orifice size were the primary independent variables. This table also gives ratios that are derived from the primary variables: the orifice to main-stream area ratio, the jet-to-total mass flow split, and the parameter coupling the spacing and momentum-flux ratio. Not all combinations of the primary variables in the table were tested; only those combinations which are within the range given for the derived variables represent conditions that are within the range of the experiments.

Examining the results in figures 5 to 17 in the context of equation (3) suggests that, in general, the empirical model provides good temperature field predictions for single-side injection when $1 < C < 5$. Similarly, good predictions are obtained for opposed inline jets provided that $0.5 < C < 2.5$. This model does not work well for impinging flows because the experimental temperature distributions are not consistent with the assumption of Gaussian profile similarity in the empirical model. The experimental profiles for conditions giving optimum mixing in opposed staggered-jet configurations are also somewhat at variance with the model assumptions; in these cases, satisfactory agreement with the data must be considered fortuitous.

A major weakness of the empirical model used here in (refs. 17 to 19) and in previous versions (refs. 4 and 5) is that the form of the correlations precludes their use for semi-confined flows (large H_0/D or S/D), single-jet flows, or flows in which it is known a priori that the primary assumptions in the model will be invalid.

Numerical

The numerical model is not subject to the inherent limitation of the empirical model regarding profile shape and confinement. Thus, three-dimensional codes can provide calculations for complex flows for which the assumptions in the empirical model are known to be invalid or outside the range of available experiments. Furthermore, numerical models provide calculations for all flow field parameters of interest, not just those that happen to have been empirically correlated.

The numerical calculations correctly show the trends which result from variation of the independent flow and geometric variables, although the results consistently exhibit too little mixing. The numerical model calculations for the slanted slots and staggered jet cases are encouraging because the experimental data for these cases show profiles that are not consistent with the primary assumptions in the empirical model.

The numerical calculations performed are shown to be grid sensitive, and false diffusion is known to be present. Uncertainties also exist in these calculations regarding the validity of turbulence model assumptions and due to unmeasured (and hence assumed) boundary conditions. The results shown here are not intended to represent the best agreement possible from numerical models at this time. Better temperature field agreement could undoubtedly have been achieved by adjusting model constants and/or inlet boundary conditions. But, since this was not necessary to satisfy the present objective of evaluating the potential of these codes vis-a-vis combustor dilution zone flow fields, and because the mean temperature was the only parameter compared, no adjustments were made.

Thus, as with previous assessments in references 14 to 16, three-dimensional calculations, such as those in this paper, should be considered as only qualitatively accurate at this time, and three-dimensional codes of this type are useful primarily in guiding design changes or in perturbation analyses. The three-dimensional code used herein, although sufficiently promising to justify further development and assessment, is not a practical tool for general engineering use in its present form. Codes with improved numerics, accuracy, and turbulence models should provide more quantitative predictions.

CONCLUSIONS

The principal conclusions from the experimental results reviewed herein are as follows:

1. Variations of momentum-flux ratio and of orifice size and spacing have a significant effect on the flow distribution.

2. Similar distributions can be obtained, independent of orifice diameter, when momentum-flux ratio and orifice spacing are coupled.

3. A first-order approximation of the mixing of jets with a variable-temperature main stream can be achieved by superimposing the jets-in-an-isothermal-main-stream and upstream profiles.

4. The penetration and mixing of jets issuing from 45° slanted slots are less than those from equivalent-area circular holes.

5. With the same orifice spacing in (at least) the lead row, double rows of jets have temperature distributions similar to those from a single row of equally spaced, equivalent-area circular orifices.

6. For opposed rows of jets, with the orifice centerlines in line, the optimum ratio of orifice spacing to duct height is one-half the optimum value for single-side injection at the same momentum-flux ratio.

7. For opposed rows of jets with the orifice centerlines staggered, the optimum ratio of orifice spacing to duct height is twice the optimum value for single-side injection at the same momentum-flux ratio.

Temperature field measurements from the experiments cited previously are compared with distributions calculated using an empirical model based on assumed vertical profile similarity and superposition and with calculations made using a three-dimensional elliptic code with a standard $k-\varepsilon$ turbulence model. The results can be summarized as follows:

Empirical model calculations provide very good results for modeled parameters within the range of experiments whenever the primary assumptions in the model are satisfied.

Three-dimensional code calculations made in this study correctly approximate the trends which result from varying the independent flow and geometric variables, but they consistently exhibit too little mixing. (The advantage of these models is that they can predict all flow field quantities, flows outside the range of experiments, or flows where empirical assumptions are invalid.) Numerical calculations should yield more quantitative predictions with improvements in numerics, accuracy, and turbulence models.

REFERENCES

1. Walker, R.E.; and Kors, D.L.: Multiple Jet Study. NASA CR-121217, 1973.

2. Holdeman, J.D.; Walker, R.E.; and Kors, D.L.: Mixing of Multiple Dilution Jets with a Hot Primary Airstream for Gas Turbine Combustors. AIAA Paper 73-1249, Nov. 1973.

3. Kamotani, Y.; and Greber, I.: Experiments on Confined Turbulent Jets in Cross Flow. NASA CR-2392, 1974.

4. Walker, R.E.; and Eberhardt, R.G.: Multiple Jet Study Data Correlations. NASA CR-134795, 1975.

5. Holdeman, J.D.; and Walker, R.E.,: Mixing of a Row of Jets with a Confined Crossflow. AIAA J., vol. 15, no. 2, Feb. 1977, pp. 243-249.

6. Cox, G.B. Jr.: Multiple Jet Correlations for Gas Turbine Engine Combustor Design. J. Eng. Power, vol. 98, no. 2, Apr. 1976, pp. 265-273.

7. Cox, G.B. Jr.: An Analytical Model for Predicting Exit Temperature Profile from Gas Turbine Engine Annular Combustors. AIAA Paper 75-1307, Sept. 1975.

8. Riddlebaugh, S.M.; Lipshitz, A.; and Greber, I.: Dilution Jet Behavior in the Turn Section of a Reverse-Flow Combustor. AIAA Paper 82-0192, Jan. 1982.

9. Khan, Z.A.; McGuirk, J.J.; and Whitelaw, J.H.: A Row of Jets in a Cross-flow. Fluid Dynamics of Jets with Application to V/STOL, AGARD-CP-308, Technical Editing and Reproduction, London, 1982, pp. 10-1 to 10-11.

10. Atkinson, K.N.; Khan, Z.A.; and Whitelaw, J.H.: Experimental Investigation of Opposed Jets Discharging Normally into a Cross-Stream. J. Fluid Mech., vol. 115, Feb. 1982, pp. 493-504.

11. Wittig, S.L.K.; Elbahar, O.M.F.; and Noll, B.E.: Temperature Profile Development in Turbulent Mixing of Coolant Jets with a Confined Hot Cross Flow. J. Engr. Gas Turbines Power, vol. 106, no. 1, Jan. 1984, pp. 193-197.

12. Holdeman, J.D.: Perspectives on the Mixing of a Row of Jets with a Confined Crossflow. AIAA Paper 83-1200, June 1983.

13. Claus, R.W.: Calculation of a Single Jet in Crossflow and Comparison with Experiment. AIAA Paper 83-0238, Jan. 1983.

14. Srinivasan, R., et al: Aerothermal Modeling Program: Phase I. (Garrett 21-4742, Garrett Turbine Engine Co.; NASA Contract NAS3-23523) NASA CR-168243, 1983.

15. Kenworthy, M.J.; Correa, S.M.; and Burrus, D.L.: Aerothermal Modeling, Phase I. NASA CR-168296, 1983.

16. Sturgess, G.J.: Aerothermal Modeling Program, Phase I. (PWA-5907-19, Pratt and Whitney Aircraft; NASA Contract NAS3-23524) NASA CR-168202, 1983.

17. Srinivasan, R.; Berenfeld, A.; and Mongia, H.C.: Dilution Jet Mixing Phase I. (Garrett-21-4302, Garrett Turbine Engine Co.; NASA Contract NAS3-22110) NASA CR-168031, 1982.

18. Srinivasan, R.; Coleman, E.; and Johnson, K.: Dilution Jet Mixing Program, Phase II. (Garrett 21-4804, Garrett Turbine Engine Co.; NASA Contract NAS3-22110) NASA CR-174624, 1984.

19. Srinivasan, R., et al: Dilution Jet Mixing, Phase III. (Garrett 21-5418, Garrett Turbine Engine Co.; NASA Contract NAS3-22110). NASA CR-174884, 1985.

20. Holdeman, J.D.; and Srinivasan, R.: Modeling of Dilution Jet Flowfields. Combustion Fundamentals Research, NASA CP-2309, 1984, pp. 175-187.

21. Holdeman, J.D.; and Srinivasan, R.: On Modeling Dilution Jet Flowfields. AIAA Paper 84-1379, June 1984.

22. Holdeman, J.D.; Srinivasan, R.; and Berenfeld, A.: Experiments in Dilution Jet Mixing. AIAA J., vol. 22, no. 10, Oct. 1984, pp. 1436-1443.

23. Holdeman, J.D., et al: Experiments in Dilution Jet Mixing - Effects of Multiple Rows and Non-circular Orifices. AIAA Paper 85-1104, July 1985.

24. Bruce, T.W.; Mongia, H.C.; and Reynolds, R.S.: Combustor Design Criteria Validation. AiResearch Manufacturing Co., AIRESEARCH-75-211682(38)-1,-2, and -3, 1979 (USARTL-TR-78-55A, B, and C) (AD-A067657, AD-A067689, AD-A066793).

25. Patankar, S.V.; and Spalding, D.B.: A Calculation Procedure for Heat, Mass and Momentum Transfer in Three-Dimensional Parabolic Flows. Int. J. Heat Mass Trans., vol. 15, no. 10, Oct. 1972, pp. 1787-1806.

26. Patankar, S.Y.; and Spalding, D.B.: A Computer Model for Three-Dimensional Flow in Furnaces. 14th Symposium (International) on Combustion, The Combustion Institute, Pittsburgh, 1973, pp. 605-614.

TABLE I. - FLOW AND GEOMETRY CONDITIONS

Figure	S/H_0	H_0/D	A_j/A_m	C_d	DR	$\sqrt{J}$	w_j/w_T	C^a
2	0.5	4	0.10	0.76	2.2	26.2	0.36	2.56
5(a), 6(a)	.25	8	.05	.60	2.1	22.4	.17	1.18
5(b), 6(b)	1.0	4	.05	.67	2.2	23.5	.19	4.85
7(a)	1.0	4	.05	.73	2.1	5.3	.11	2.30
7(b), 14(a)	.5	8	.025	.61	2.2	28.4	.11	2.66
7(c)	.25	8	.05	.61	2.3	92.7	.30	2.60
8(a)	.5	5.7	.05	.71	2.2	25.4	.21	2.52
8(b), 9(a), 16(a)	.5	4	.10	.61	2.1	18.6	.27	2.16
[b]9(b), 10	.5	4	.10	.61	1.8	31.3	.31	2.80
[c]9(c)	.5	4	.10	.68	2.2	24.4	.31	2.47
[d]11	.5	4	.10	.66	2.2	27.1	.33	2.60
12	.5	5.7	.05	.65	2.2	26.3	.33	2.56
	.5	5.7	.05	.66	2.2	26.9	----	2.59
13	.5	5.7	.05	.69	2.2	26.8	.34	2.59
	.25	8	.05	.70	2.2	26.6	----	1.29
14(b), 15	.25	8	.10	.65	2.1	25.0	.32	1.25
16(b), 17	1.0	4	.10	.65	2.1	27.6	.33	5.25

[a]$C = (S/H_0)\sqrt{J}$.
[b]Top cold.
[c]Top hot.
[d]45° slanted slots.

TABLE II. - SPACING AND MOMENTUM-FLUX RATIO RELATIONS

Configuration	$C = (S/H_0)\sqrt{(J)}$
Single-side injection	
Underpenetration	<1.25
Optimum	2.5
Overpenetration	>5
Opposed rows of jets	
Inline optimum	1.25
Staggered optimum	5

TABLE III. - RANGE OF INDEPENDENT FLOW AND GEOMETRIC VARIABLES INVESTIGATED IN REFERENCES 17 TO 19

DR	0.5 to 2.5
J	5 to 105
S/H_0	0.125 to 1
H_0/D	4 to 16
A_j/A_m	0.025 to 0.1
w_j/w_T	0.075 to 0.33
$C = (S/H_0)\sqrt{J}$	0.5 to 10

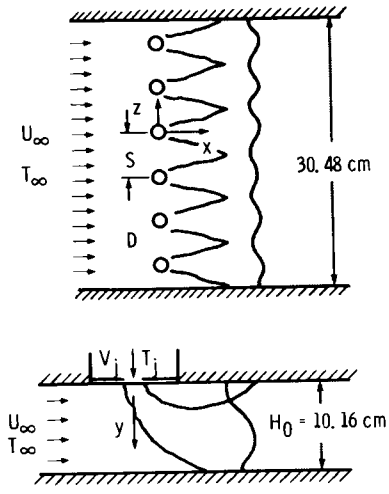

Figure 1. - Schematic of multiple jet flow.

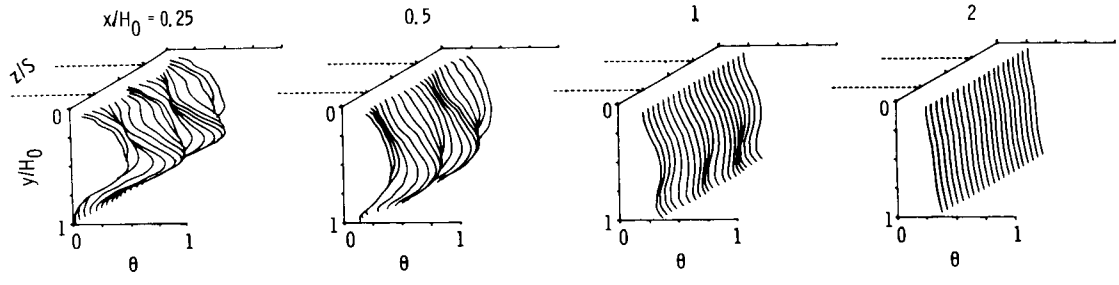

Figure 2. - Experimental mean temperature distributions (J = 26.2, S/H_0 = 0.5, H_0/D = 4).

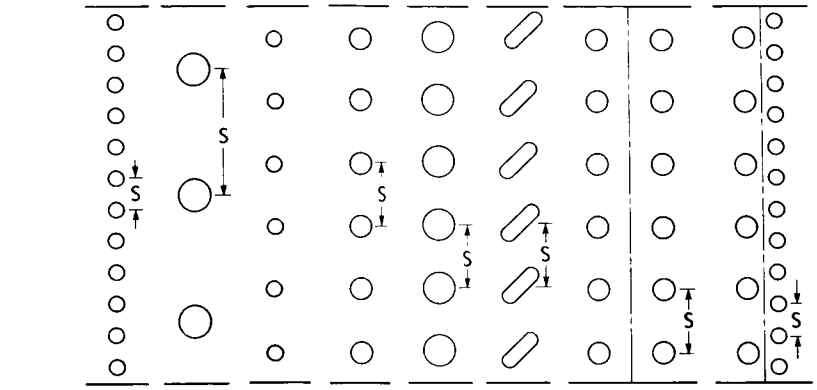

Figure 3. - Dilution-jet mixing orifice configurations.

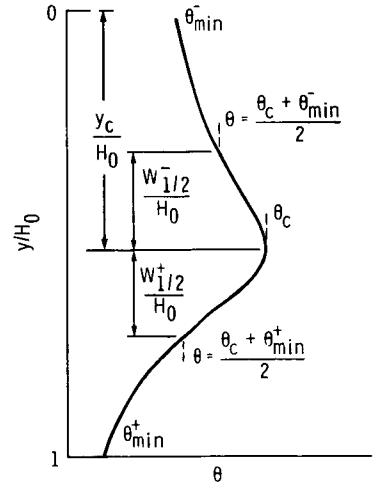

Figure 4. - Schematic of typical vertical temperature profile showing scaling parameters in empirical model.

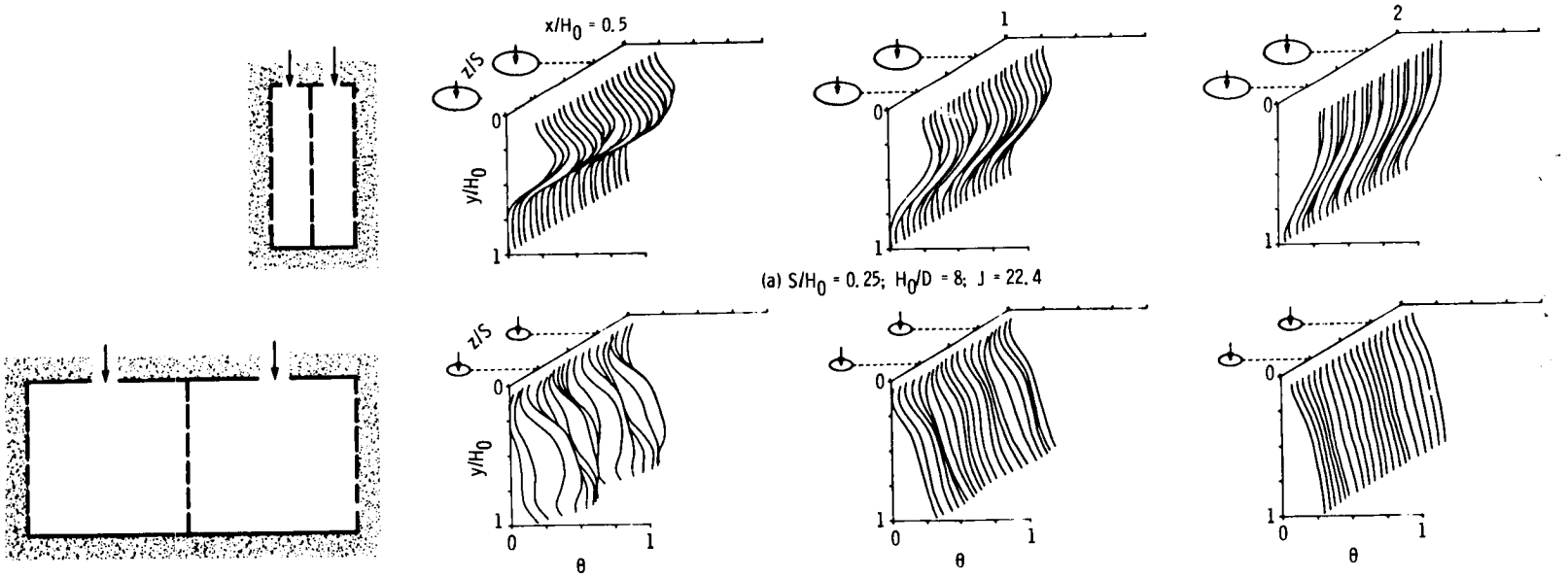

Figure 5. - Effect on temperature distributions of varying orifice spacing at constant area (A_j/A_m = 0.05).

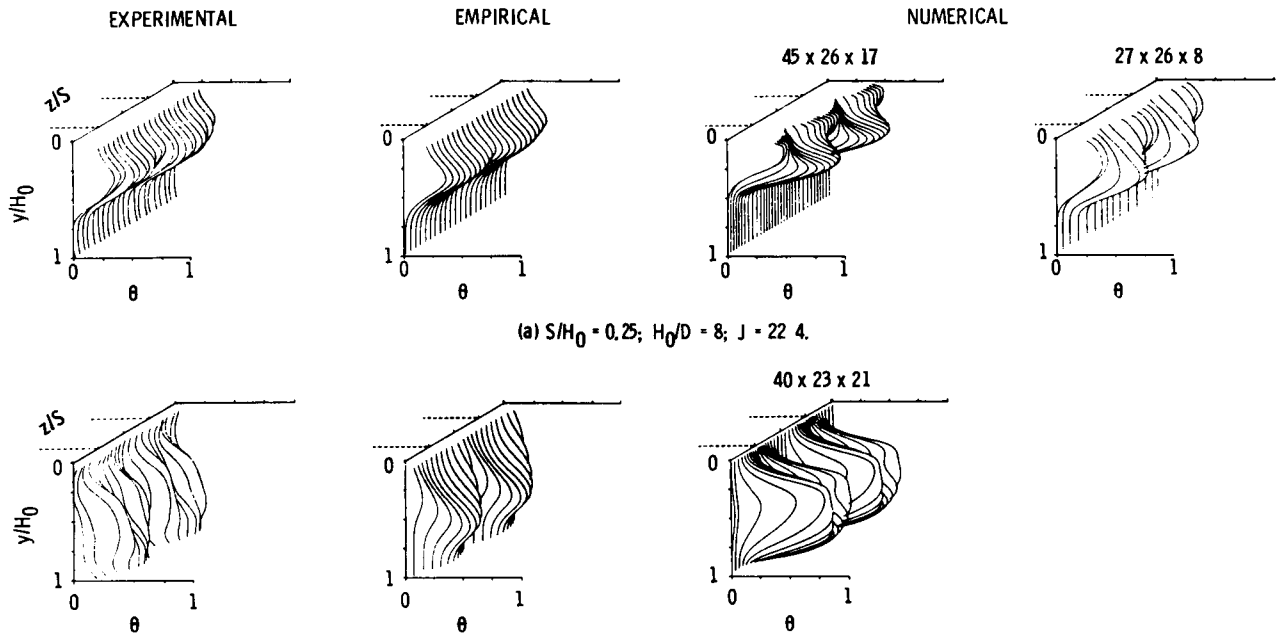

(a) $S/H_0 = 0.25$; $H_0/D = 8$; $J = 22.4$.

(b) $S/H_0 = 1$; $H_0/D = 4$; $J = 23.5$.

Figure 6. - Effect of varying orifice spacing at constant area on measured and calculated temperature distributions when $x/H_0 = 0.5$ ($A_j/A_m = 0.05$).

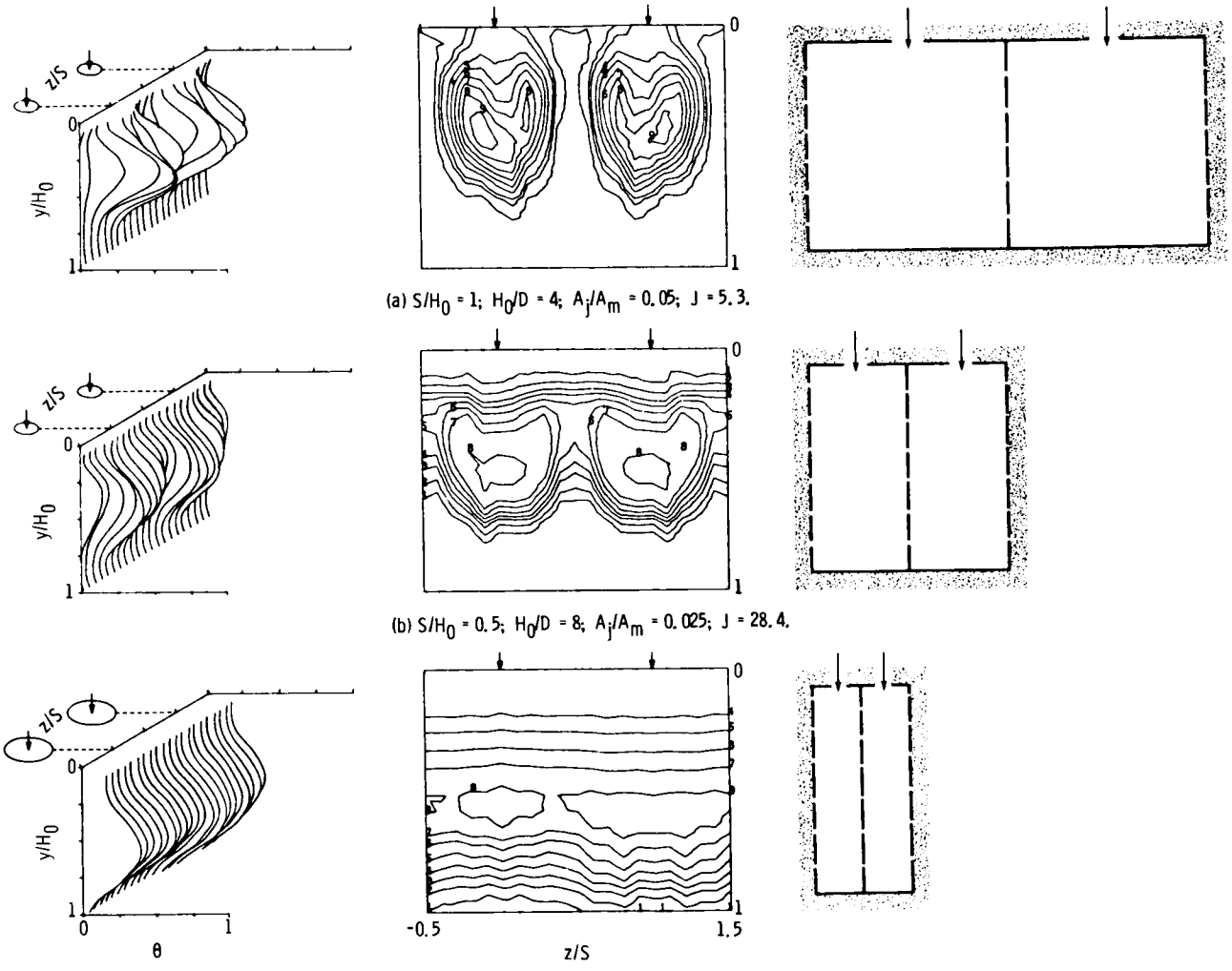

Figure 7. - Oblique profile plots and isotherm contours when $x/H_0 = 0.5$ for coupled orifice spacing and momentum-flux ratio.

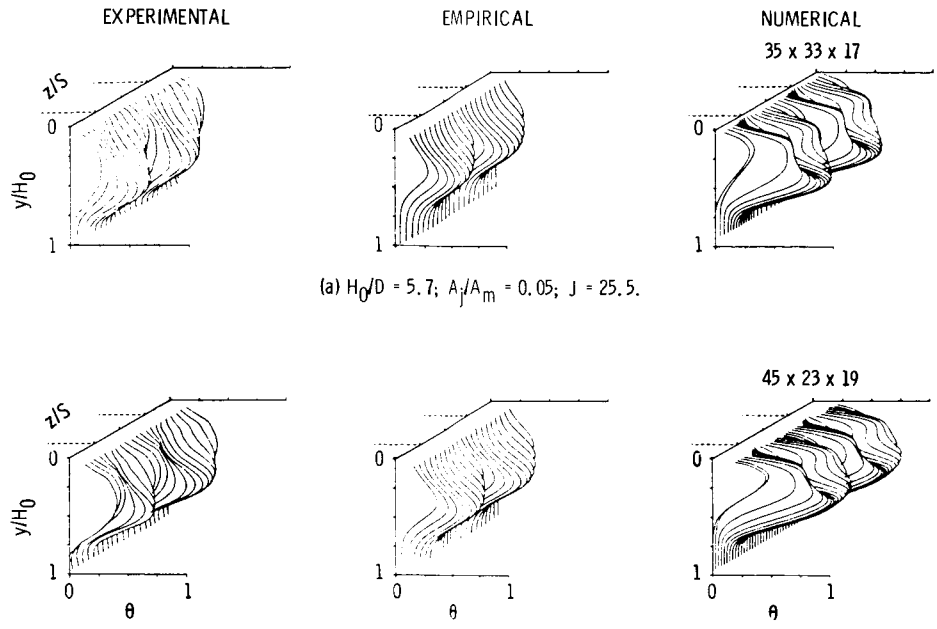

(a) $H_0/D = 5.7$; $A_j/A_m = 0.05$; $J = 25.5$.

(b) $H_0/D = 4$; $A_j/A_m = 0.10$; $J = 18.6$.

Figure 8. - Effect of varying orifice diameter at constant spacing on measured and calculated temperature distributions when $x/H_0 = 0.5$ ($S/H_0 = 0.5$).

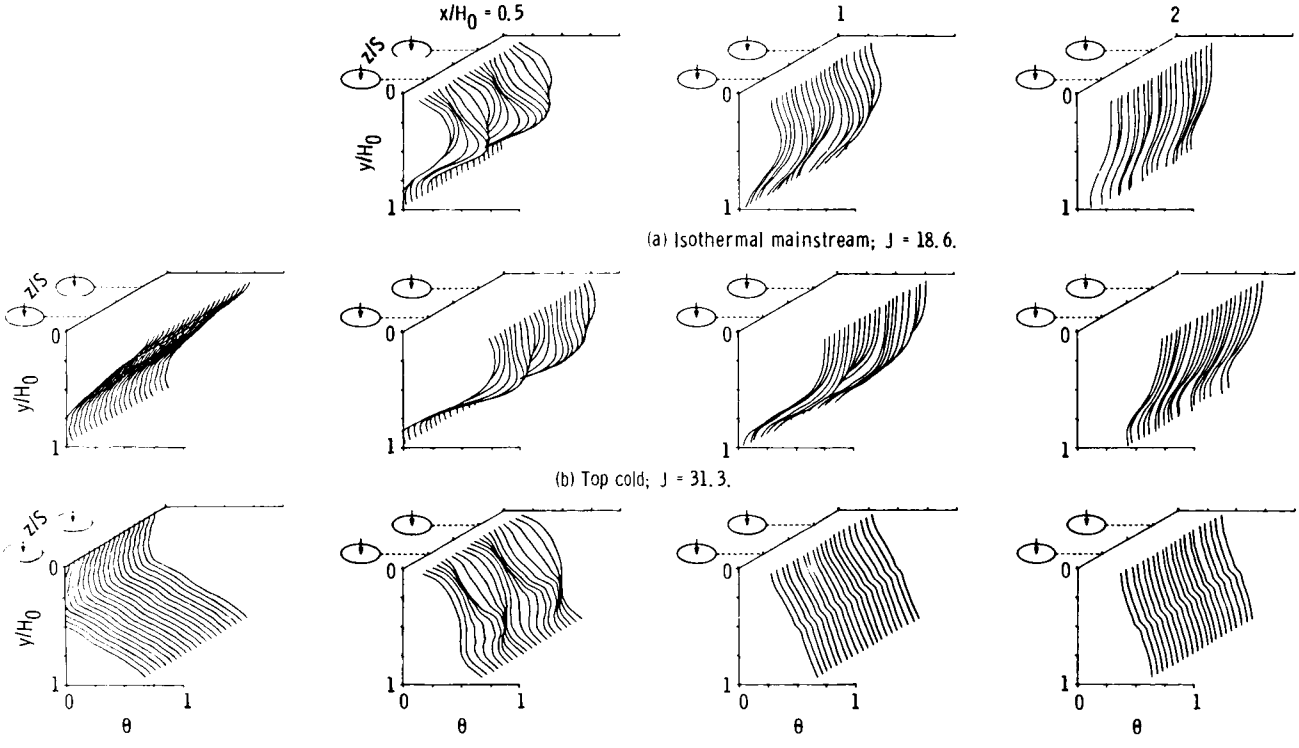

(a) Isothermal mainstream; $J = 18.6$.

(b) Top cold; $J = 31.3$.

(c) Top hot; $J = 24.4$.

Figure 9. - Influence of nonisothermal mainstream on measured temperature profiles ($S/H_0 = 0.5$; $H_0/D = 4$, $A_j/A_m = 0.10$).

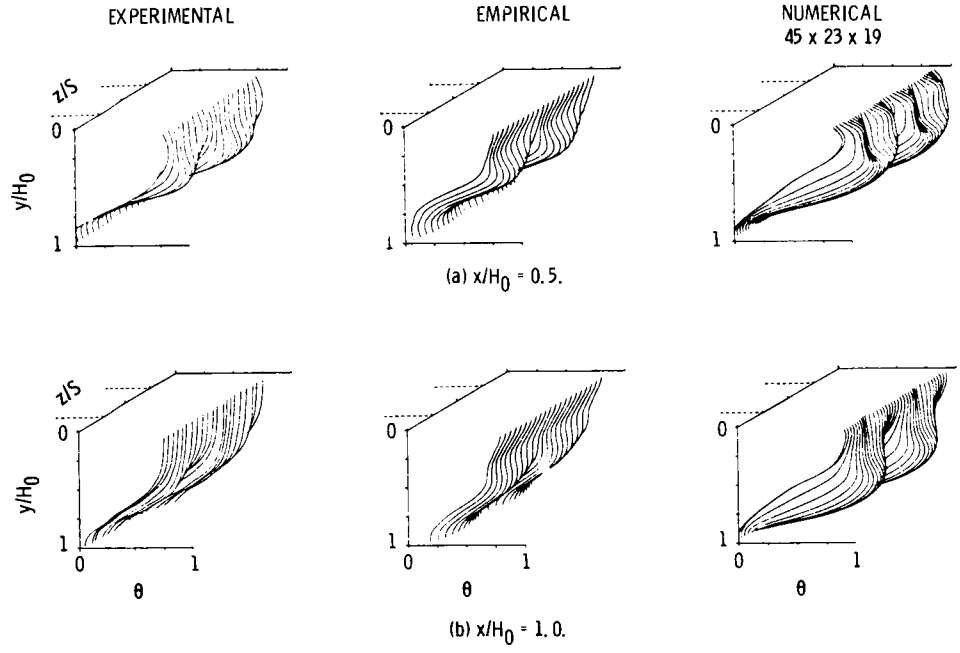

Figure 10. - Measured and calculated temperature distribution for jets injected into a nonisothermal mainstream; top cold ($S/H_0 = 0.5$, $H_0/D = 4$, $J = 31.3$).

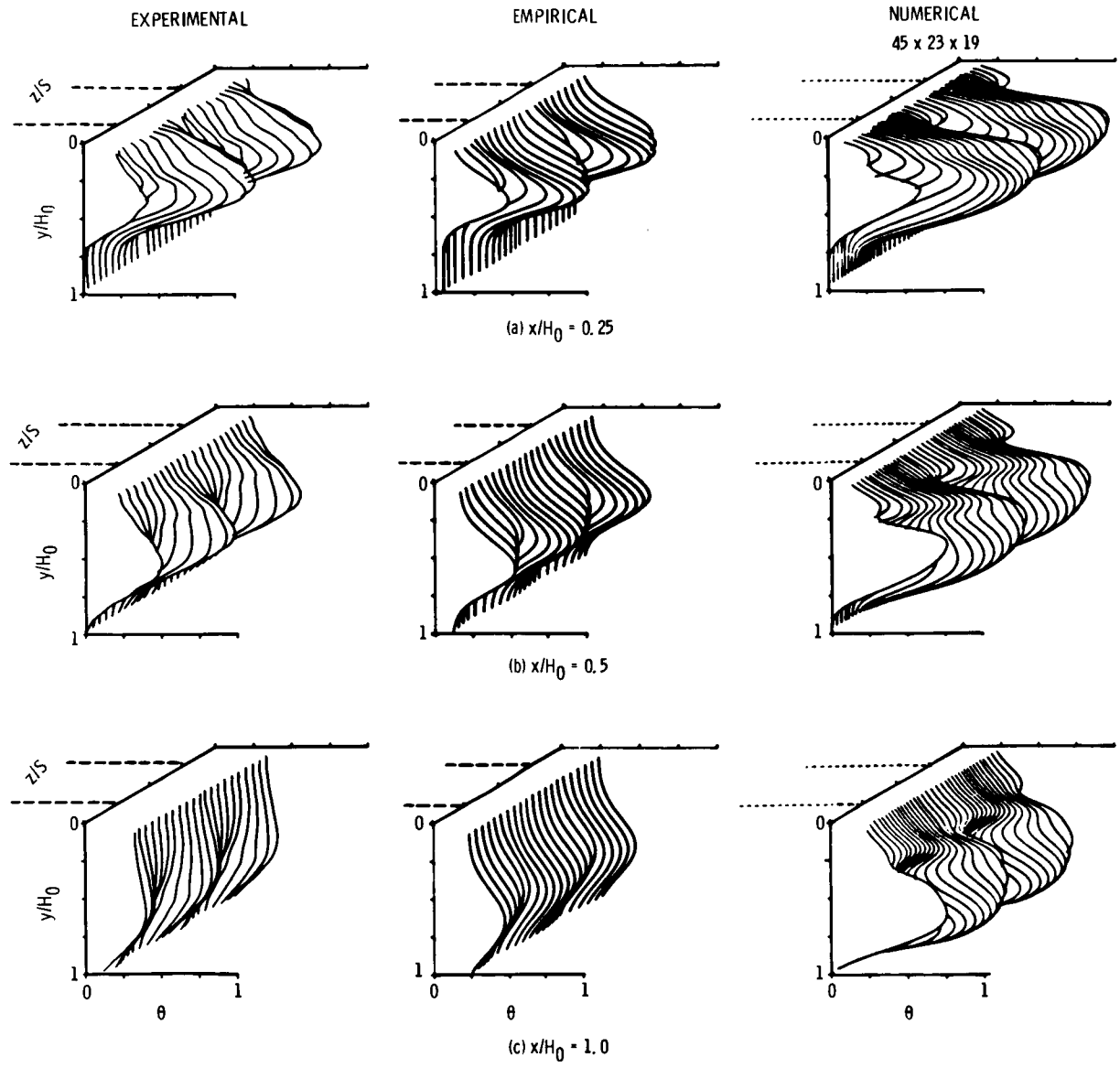

Figure 11. - Measured and calculated temperature distributions for slanted slots at an intermediate momentum-flux ratio ($S/H_0 = 0.5$, $H_0/D = 4$, $J = 27.1$).

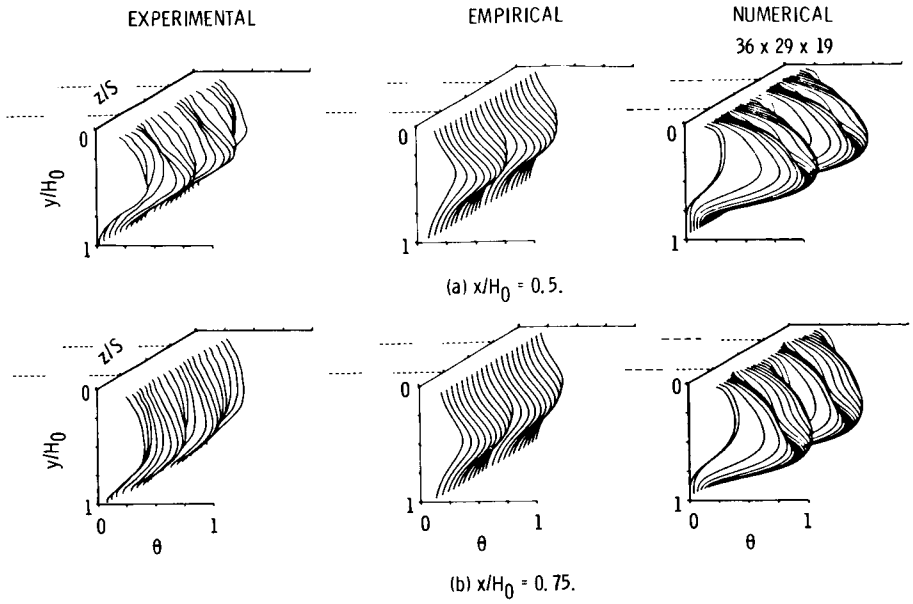

Figure 12. - Measured and calculated temperature distributions for double row of inline jets at an intermediate momentum-flux ratio (A_j/A_m = 0.10, S_x/H_0 = 0.5. Row 1: S/H_0 = 0.5, H_0/D = 5.7, J = 26.3. Row 2: S/H_0 = 0.5, H_0/D = 5.7, J = 26.9).

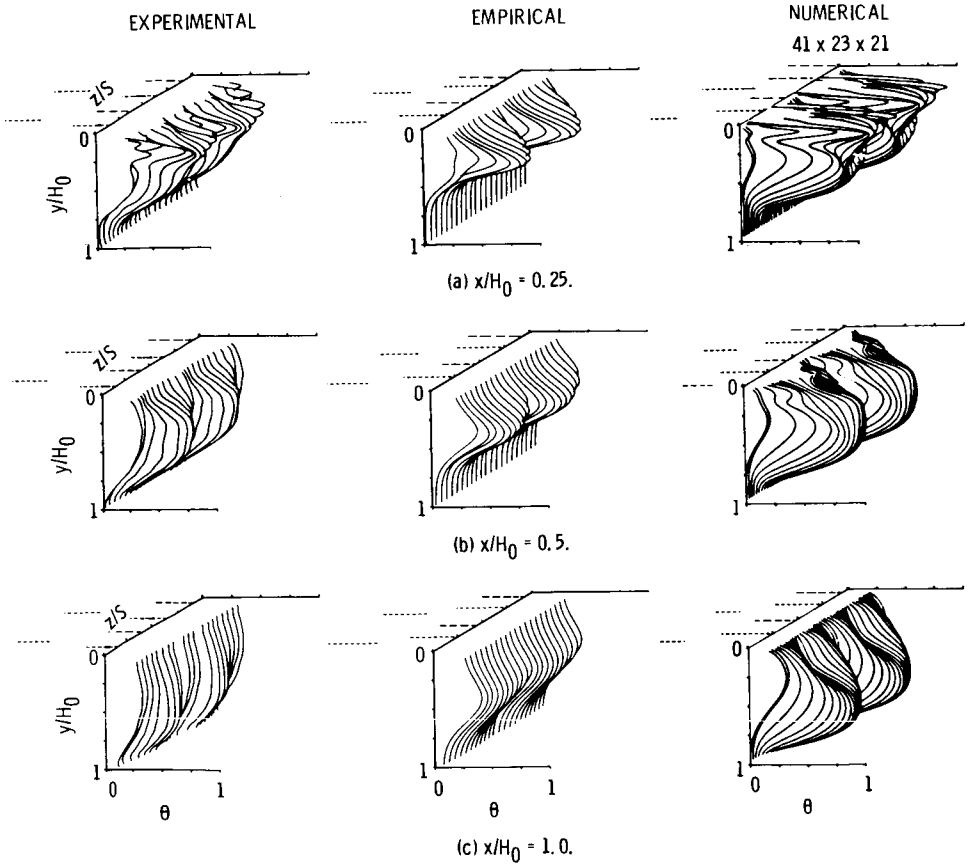

Figure 13. - Measured and calculated temperature distributions for double row of dissimilar jets at an intermediate momentum-flux ratio (A_j/A_m = 0.10, S_x/H_0 = 0.25. Row 1: S/H_0 = 0.5, H_0/D = 5.7, J = 26.8. Row 2: S/H_0 = 0.25, H_0/D = 8, J = 26.6).

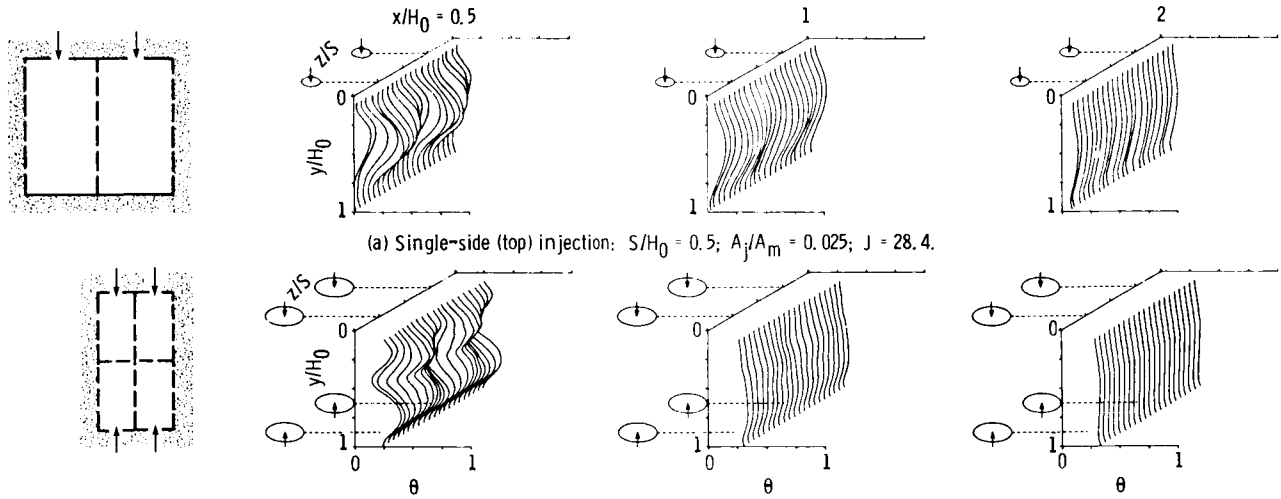

(a) Single-side (top) injection: $S/H_0 = 0.5$; $A_j/A_m = 0.025$; $J = 28.4$.

(b) Opposed row (inline) injection: $S/H_0 = 0.25$; $A_j/A_m = 0.10$; $J = 25.0$.

Figure 14. - Comparison between single-side and opposed-jet injection ($H_0/D = 8$).

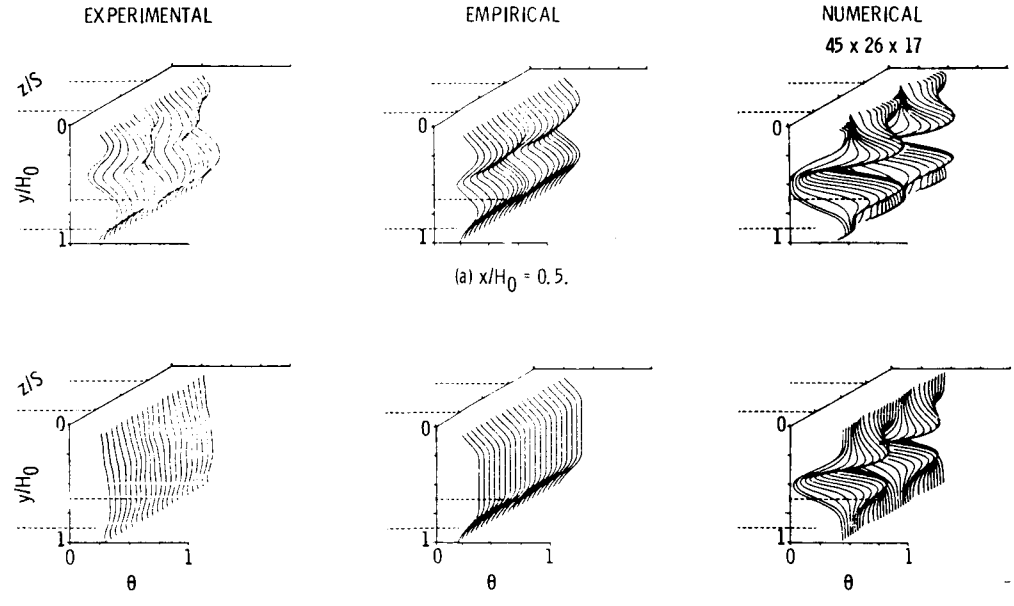

(a) $x/H_0 = 0.5$.

(b) $x/H_0 = 1.0$.

Figure 15. - Measured and calculated temperature distributions for opposed rows of inline jets ($S/H_0 = 0.25$, $H_0/D = 8$, $A_j/A_m = 0.10$, $J = 25$).

ORIGINAL PAGE IS
OF POOR QUALITY

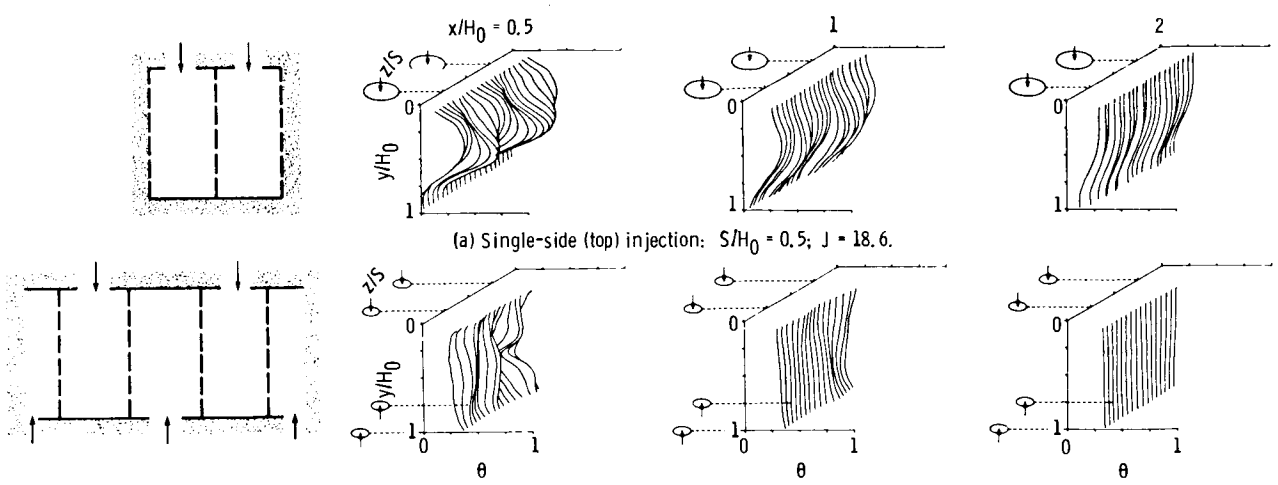

(a) Single-side (top) injection: $S/H_0 = 0.5$; $J = 18.6$.

(b) Opposed row (staggered) injection: $S/H_0 = 1$; $J = 27.6$.

Figure 16. - Comparison between single-side and staggered jet injection ($H_0/D = 4$, $A_j/A_m = 0.10$).

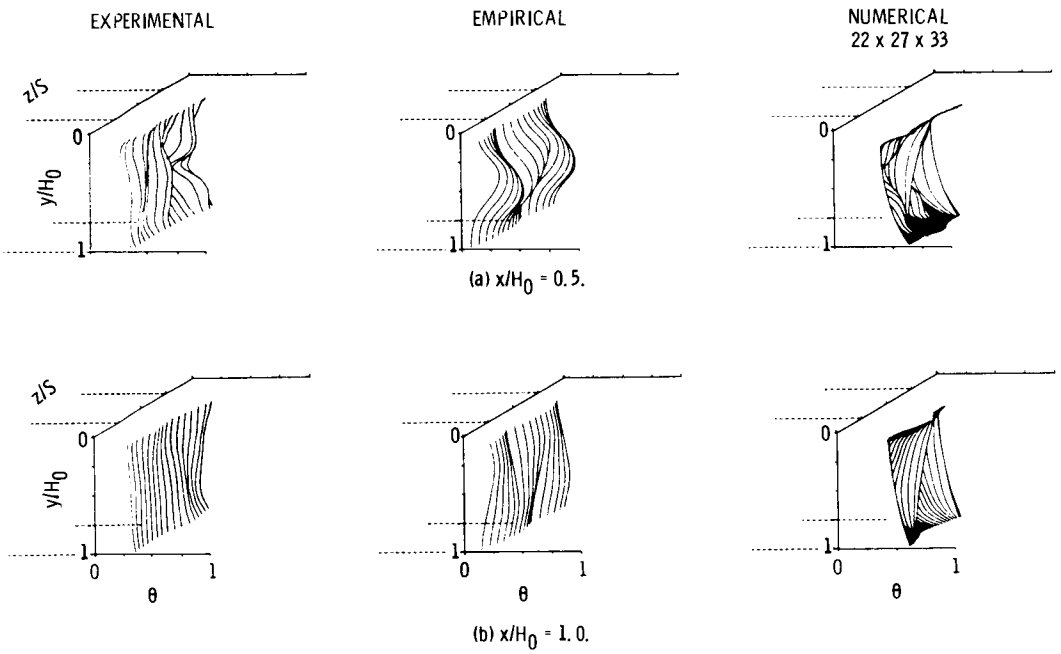

(a) $x/H_0 = 0.5$.

(b) $x/H_0 = 1.0$.

Figure 17. - Measured and calculated temperature distributions for opposed rows of staggered jets ($S/H_0 = 1$, $H_0/D = 4$, $A_j/A_m = 0.10$, $J = 27.6$).